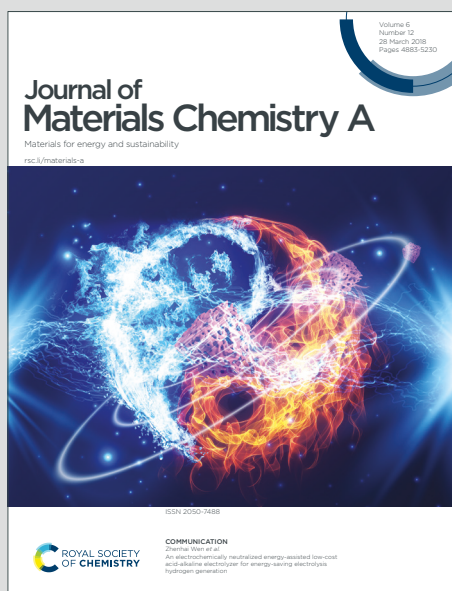


# Journal of Materials Chemistry A

Materials for energy and sustainability

Accepted Manuscript

This article can be cited before page numbers have been issued, to do this please use: C. Zhong, Y. Xiao, J. Feng, C. Liu, L. Li, W. F. Ip, S. Wang and H. Pan, *J. Mater. Chem. A*, 2025, DOI: 10.1039/D4TA08772K.



This is an Accepted Manuscript, which has been through the Royal Society of Chemistry peer review process and has been accepted for publication.

Accepted Manuscripts are published online shortly after acceptance, before technical editing, formatting and proof reading. Using this free service, authors can make their results available to the community, in citable form, before we publish the edited article. We will replace this Accepted Manuscript with the edited and formatted Advance Article as soon as it is available.

You can find more information about Accepted Manuscripts in the [Information for Authors](#).

Please note that technical editing may introduce minor changes to the text and/or graphics, which may alter content. The journal's standard [Terms & Conditions](#) and the [Ethical guidelines](#) still apply. In no event shall the Royal Society of Chemistry be held responsible for any errors or omissions in this Accepted Manuscript or any consequences arising from the use of any information it contains.

## COMMUNICATION

## Revealing the hydrogen bond network effect at electrode-electrolyte interface during hydrogen evolution reaction

Chengcheng Zhong,<sup>a</sup> Yuxuan Xiao,<sup>\*a</sup> Jinxian Feng,<sup>a</sup> Chunfa Liu,<sup>a</sup> Lun Li,<sup>a</sup> Weng Fai IP,<sup>b</sup> Shuangpeng Wang<sup>\*a</sup> and Hui Pan<sup>\*a,b</sup>Received 00th January 20xx,  
Accepted 00th January 20xx

DOI: 10.1039/x0xx00000x

**The hydrogen bond network (HBN) in the electrical double layer (EDL) at the electrode-electrolyte interface plays a crucial role in governing water migration, which directly affects the efficiency of hydrogen evolution reaction. However, existing research has primarily focused on the connectivity of the HBN within the inner Helmholtz layer, often neglecting the water transport across the entire EDL. In this study, we develop a high-performance Aermet100 steel-derived catalyst, which achieves an overpotential of 307 mV for the hydrogen evolution reaction at a current density of 500 mA cm<sup>-2</sup> under industrial conditions. Using this catalyst, we investigate the migration of water in KOH solutions with varying concentrations. Our findings show that water migration is inhibited in 1 M KOH due to the relatively stronger HBN, whereas it is enhanced in 3 M and 6 M KOH solutions. These results provide new insights into the kinetics of water transport and offer a potential pathway for optimizing industrial water electrolysis processes.**

Green hydrogen is increasingly poised to replace traditional fossil fuels due to its cleanness and renewability.<sup>1-3</sup> Currently, water electrolysis has been recognized as an efficient technology to produce green hydrogen with high purity. Therefore, extensive research has been focused on enhancing the efficiency of the catalysts for water electrolysis.<sup>4</sup> Noble metals such as platinum (Pt)-based and ruthenium (Ru)-based materials are acknowledged as the best electrocatalysts for the cathodic hydrogen evolution reaction (HER) and anodic oxygen evolution reaction (OER), respectively, in water electrolysis because of their exceptional capacity to adsorb and recombine the reaction intermediates.<sup>5-7</sup> However, their low storage, high

cost and inadequate durability have restricted the practical application. Instead, developing non-precious transition metal-based materials as catalysts for industrially applicable water electrolysis is of great interest, because the transition metal-based materials have shown promising performance due to their high affinity to water molecules.<sup>8-20</sup>

In parallel with the design of high-performance transition metal-based catalysts, understanding the mechanism of water electrolysis, particularly in the region of the electrical double layer (EDL) is significant. The EDL consists of the inner Helmholtz plane (IHP), outer Helmholtz plane (OHP), and the diffusion layer.<sup>18</sup> The connectivity of the hydrogen bond network (HBN) in the inner Helmholtz layer (IHP), as described in the HBN theory, has attracted significant attention as an important index for evaluating catalytic efficiency.<sup>21-26</sup> The HBN connectivity can regulate the kinetics of interfacial proton-coupled electron transfer reactions, thereby affecting the performance of water electrolysis.<sup>19,23</sup> However, little attention has been taken to the effect of HBN on the transport of water molecules throughout the entire EDL. The timely transport of water molecules to the electrode surface as reactants, facilitated by the breaking of the HBN, is essential for efficient hydrogen evolution.

Herein, the migration of water molecules influenced by the HBN is thoroughly investigated. Industrial-grade Aermet100 (A100) steel was electrochemically treated in-situ to form metal hydroxides on its surface in KOH solution. The A100 treated in 6 M KOH (referred to as A100-6) exhibited the best water electrolysis performance under both laboratory and industrial conditions. In-situ Raman and Fourier-transform infrared (FTIR) spectroscopies were employed to explore the distinct effects of the HBN on the mobility of water molecules at the electrolyte-electrode interface across varying concentrations of KOH electrolytes.

<sup>a</sup> Institute of Applied Physics and Materials Engineering, University of Macau, Macao SAR, China.<sup>b</sup> Department of Physics and Chemistry, Faculty of Science and Technology, University of Macau, Macao SAR, China.

† Electronic supplementary information (ESI) available.



## COMMUNICATION

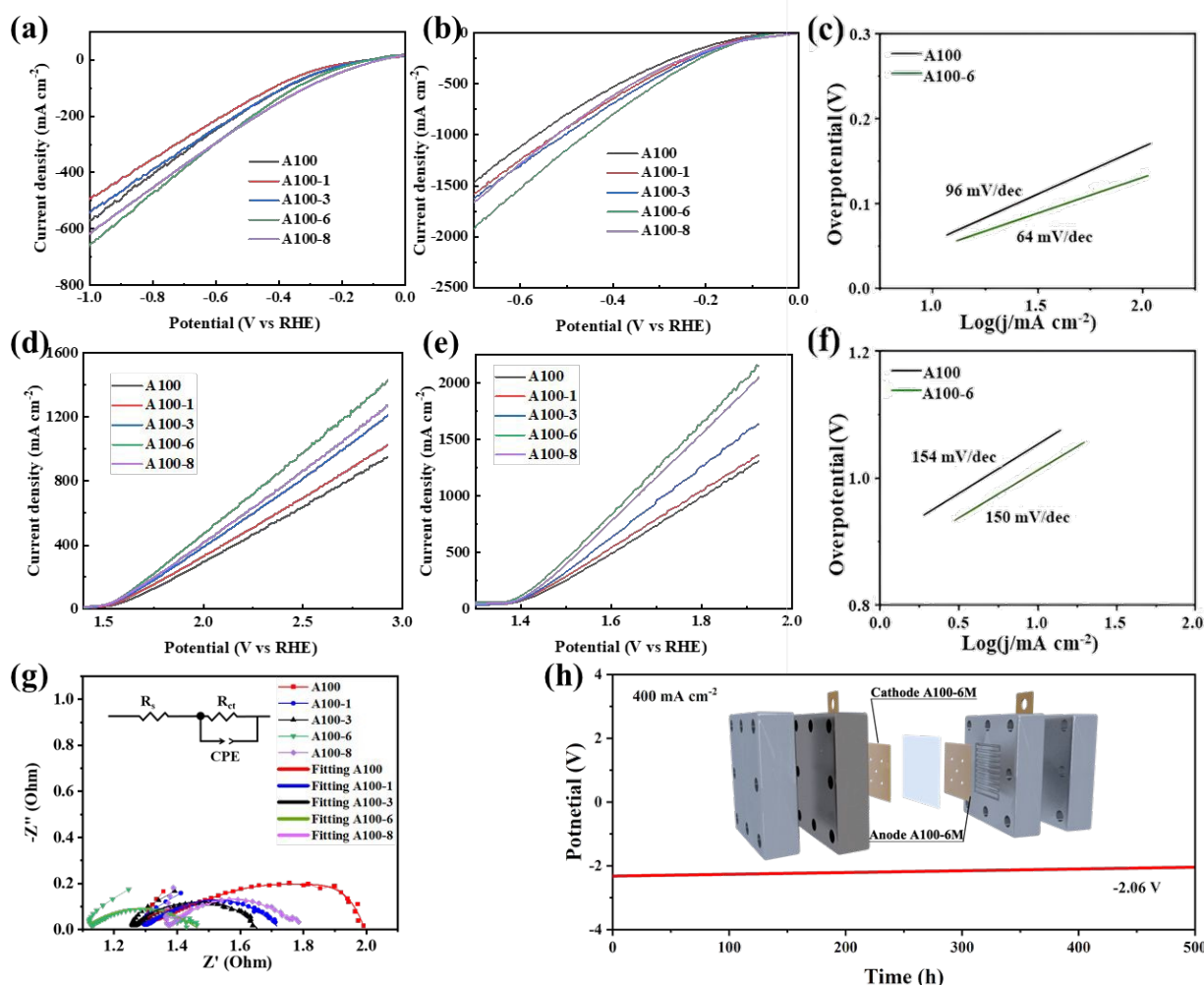


**Fig. 1** The electrochemical tests of catalysts. The HER polarization curves of treated and untreated A100 in (a) laboratory condition (1 M KOH and ambient temperature) and (b) industrial condition (6 M KOH and 60 °C). (c) Tafel slopes of A100 and A100-6 in industrial condition. The OER polarization curves of treated and untreated A100 in (d) laboratory condition and (e) industrial condition. (f) Tafel slopes of A100 and A100-6 in industrial condition. (g) Nyquist plots and equivalent circuit of treated and untreated A100 in laboratory condition. (h) Chrono voltage measurement at the current density of 400 mA cm<sup>-2</sup> of A100-6 by flow cell in industrial condition.

Water electrolysis performances of treated and untreated A100 were first evaluated. Fig. 1a and b show the cathodic HER performances of the treated and untreated A100 in laboratory

(1M KOH, ambient temperature) and industrial conditions (6 M KOH, 60 °C), respectively. Obviously, A100-6 exhibits larger current density than other samples at the same potential in



both laboratory and industrial conditions. The overpotentials of A100-6 to drive a current density of  $500 \text{ mA cm}^{-2}$  are 830 mV and 305 mV in laboratory and industrial conditions, respectively, which are much lower than those of A100 (910 mV and 395 mV) and A100 treated in 1 M (denoted as A100-1, 1000 mV and 350 mV), 3 M (denoted as A100-3, 950 mV and 330 mV) and 8 M KOH (denoted as A100-8, 860 mV and 370 mV). At same time, both HER and OER performance of A100-6 is higher than that of commercial nickel net (Fig. S13), indicating a high potential of industrial water splitting application for this cost-effective material derived from industrial steel. Moreover, A100-6 also exhibits a smaller Tafel slope ( $64 \text{ mV dec}^{-1}$ ) than that of A100 ( $96 \text{ mV dec}^{-1}$ ), indicating the improvement of reaction kinetics after treating A100 in 6 M KOH (Fig. 1c). Tafel slope values of 120, 40, and  $30 \text{ mV dec}^{-1}$  are corresponding to the Volmer, Heyrovsky, and Tafel reactions of catalysts, respectively.<sup>27</sup> Based on the observed Tafel slopes, it can be indicated that the HER process for A100 is primarily controlled by the Volmer step, indicating that water dissociation and electron transfer are the rate-determining steps. In contrast, for A100-6, the HER process appears to be under mixed control involving both the Volmer and Heyrovsky steps, suggesting a balance between water dissociation and hydrogen adsorption-desorption kinetics. Electrochemical impedance spectroscopy (EIS) results further reveal that A100-6 has the smallest charge transfer resistance (Fig. 1g), which explains its best HER performance and the corresponding equivalent circuit were also shown. The  $R_s$ ,  $R_{ct}$  and CPE represent solution resistance, charge transfer resistance of  $R_{ct}$ , respectively.<sup>28</sup> In addition, the anodic OER performances of the catalysts were also studied. Similar to the HER results, A100-6 exhibits the largest current density among all the samples in both laboratory and industrial conditions, as well as a smaller Tafel slope than A100. The stability of water electrolysis for A100-6 under industrial condition was further evaluated using a flow cell. The stability of water electrolysis for A100-6 under industrial conditions was further evaluated using a flow cell. As shown in Fig. 1h, after 500 hours of cycling tests at a current density of  $400 \text{ mA cm}^{-2}$ , the cell potential was decreased from  $-2.3 \text{ V}$  to  $-2.06 \text{ V}$ , demonstrating good stability. The schematic illustration of the in-situ treatment of industrial A100 steel and the corresponding cyclic voltammetry (CV) curves are shown in Fig. S1 (ESI<sup>†</sup>). Scanning electron microscopy (SEM) was utilized to characterize the surface morphology of A100-6. As the SEM image in Fig. S2a (ESI<sup>†</sup>), shows that numerous nanoparticles appear on the

surface of A100 following the treatment, which is far different from the smooth surface of A100 (Fig. S3a, ESI<sup>†</sup>). The corresponding X-ray energy dispersive spectroscopy (EDS) results show that the Fe is dominant in both A100 and A100-6, with small portions of Co, Ni, Cr and Mo (Fig. S2b, Fig. S3b, ESI<sup>†</sup>). The metal content dissolved in electrolyte after the treatment is characterized by inductively coupled plasma mass spectrometer (ICP-MS). The results show that an increased dissolution amount for Ni, Co and Fe with the increased KOH treatment concentration (Fig. S4, ESI<sup>†</sup>). However, decreased dissolution ratios of Cr and Mo can be found following the increased KOH concentration, which is due to their relatively stronger anti-corrosion property than Ni, Co and Fe. Moreover, the X-ray diffraction (XRD) patterns of treated and untreated A100 indicate that  $\alpha$ -Fe, characterized by a less compact lattice structure and higher surface activity, dissolves during electrochemical treatment, while  $\gamma$ -Fe, known for its stability,<sup>29</sup> is retained in greater amounts (Fig. S5, ESI<sup>†</sup>).

The surface chemical states of samples were further analysed by X-ray photoelectron spectroscopy (XPS). The XPS survey spectra of A100, A100-6 and A100-6 after durability test are shown in Fig. S6 (ESI<sup>†</sup>). The high-resolution core levels XPS spectra show similar chemical states of Fe, Co, Ni and Cr elements for A100-6 and A100 (Fig. S7a-d and Fig. S8a-d, ESI<sup>†</sup>). However, the previously undetectable Mo signal in A100 emerges in the XPS spectra of A100-6 (Fig. S7e and Fig. S8e, ESI<sup>†</sup>). This phenomenon can be attributed to surface dissolution during KOH treatment, exposing the inner Mo content of A100. Moreover, A100-6 exhibits a much higher ratio of M-OH/M-O species (Fig. S7f, ESI<sup>†</sup>) than that of A100 (Fig. S8f, ESI<sup>†</sup>), illustrating an enhanced metal hydroxide amount formed on the surface on A100 after treatment. After the durability test, the oxidation states of the metal elements increase (Fig. S9a-e, ESI<sup>†</sup>), while the M-OH/M-O ratio decreases (Fig. S9f, ESI<sup>†</sup>), indicating a consumption of surface metal hydroxide during the electrocatalytic process.

The ultraviolet photo-electron spectroscopy (UPS) analysis was conducted to investigate the work functions (WFs) of samples (Fig. S10a-e, ESI<sup>†</sup>). The results indicate the WFs of A100, A100-1, A100-3, A100-6 and A100-8 are 3.86, 3.07, 2.60, 2.23 and 2.26 eV, respectively (Fig. S10f, ESI<sup>†</sup>). A lower WF value indicates a reduced energy barrier for electron transfer at the material surface.<sup>30</sup> This could explain that A100-6 with a lowest WF value exhibits the highest HER performance than the other samples.



## COMMUNICATION

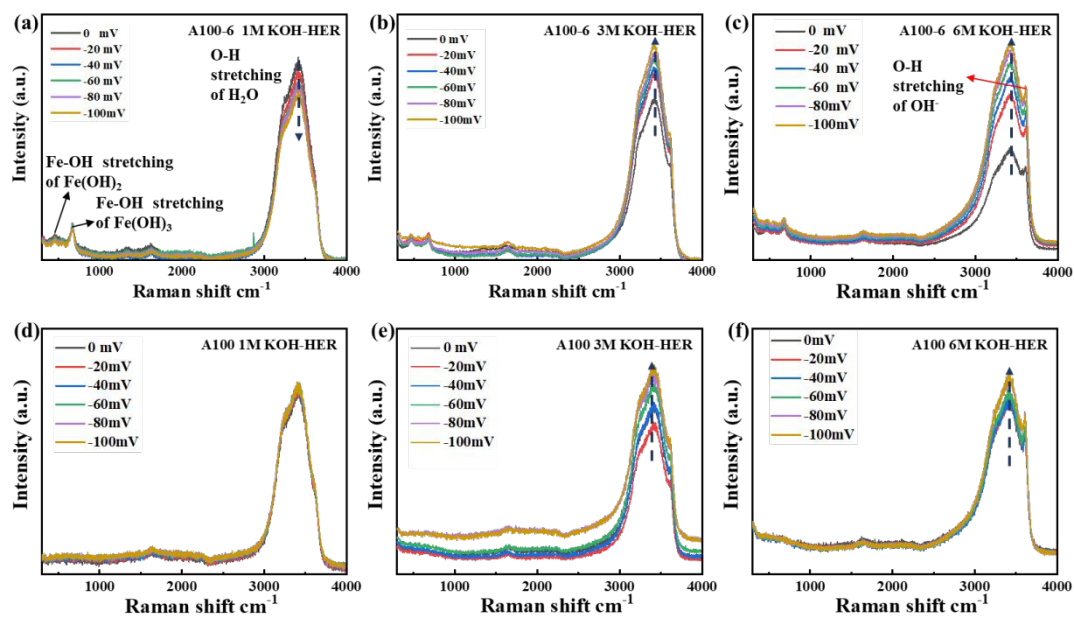


**Fig 2.** In-situ Raman spectra (HER process) of A100-6 in (a) 1M KOH, (b) 3 M KOH and (c) 6 M KOH. In-situ Raman spectra (HER process) of A100 in (d) 1M KOH, (e) 3 M KOH and (f) 6 M KOH solution at different overpotentials.



## COMMUNICATION

To systematically investigate the electrode-electrolyte interactions during water electrolysis and elucidate the underlying mechanism, in-situ Raman spectroscopy was conducted on A100 and A100-6 in KOH solutions with varying concentration (1 M, 3 M and 6 M). The in-situ Raman spectra of A100 and A100-6 for HER process are shown in Fig. 2. For A100-6, the bands at  $\sim 473$  and  $\sim 680$   $\text{cm}^{-1}$  are attributed to the Fe-OH stretching of  $\text{Fe}(\text{OH})_2$  and  $\text{Fe}(\text{OH})_3$ , which are in accordance with the previously reported results.<sup>31</sup> Moreover, an obvious peak appears at the range between 3000 and 3700  $\text{cm}^{-1}$  for both A100-6 and A100, which corresponds to the behaviour of the electrolyte.<sup>32</sup> As can be clearly seen, a prominent peak emerges at approximately 3600  $\text{cm}^{-1}$  with the increase of KOH concentration. The peak fitting results (Fig. S11, ESI<sup>†</sup>) indicate that three peaks at around 3250, 3450 and 3600  $\text{cm}^{-1}$  are corresponding to the O-H stretching vibration in water molecules, O-H stretching vibration in water molecules with strong hydrogen bonding, and O-H stretching vibration in  $\text{OH}^-$ ,

respectively.<sup>32</sup> The distinct spectral features of these vibration bands render them effective probes for investigating the kinetic behaviour of water molecules.

In 1 M KOH under HER process, it is noteworthy that the intensities of water peaks for A100-6 exhibit a decreased trend (Fig. 2a), while A100 exhibits a seldom changed one (Fig. 2d). In 3 M and 6 M KOH, both increased trends can be found for A100-6 and A100. Furthermore, for A100-6, the peaks of the O-H stretching vibrations are shifted to lower wave numbers with increasing voltage in both 1 M KOH and 6 M KOH (Fig. S11a and b, ESI<sup>†</sup>). However, for A100, the position of the O-H stretching peak is essentially unchanged in 1 M KOH and shows a tendency to shift to lower wave numbers in 6 M KOH (Fig. S11c and d, ESI<sup>†</sup>). Such different trends in the peak intensity and peak position for A100-6 and A100 could be owing to the different HBN effects and different interactions between electrode and water, respectively.

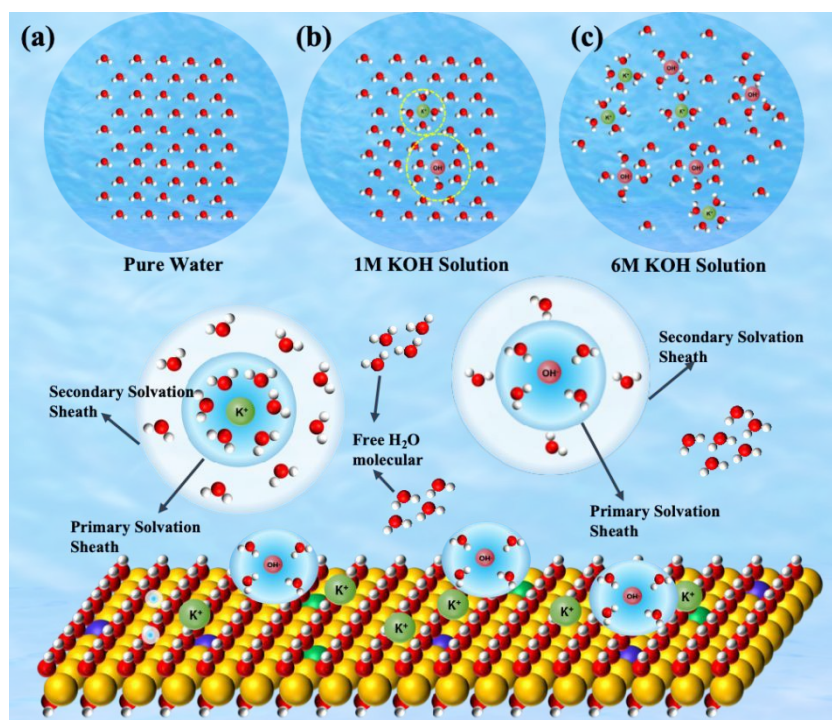


**Fig 3.** Schematic illustration of water migration as affected by HBN on the surface of A100-6. Schematic illustration of HBN in (a) pure water, (b) 1 M KOH and (c) 6 M KOH

To fully understand the HBN effect and the electrode-electrolyte interaction for A100-6 and A100 in different KOH electrolytes, we present a schematic mechanism shown in Fig. 3. As

is well established, water molecules shall usually form a network due to hydrogen bonds (Fig. 3a). However, with the addition of KOH, this network can be disrupted owing to the solvation effects of  $\text{K}^+$  and



$\text{OH}^-$ .  $\text{K}^+$  typically binds with 6–8 water molecules through ion-dipole interactions, while  $\text{OH}^-$  usually binds with 3–4 water molecules through strong hydrogen bonds.<sup>27</sup> This suggests that the migration of water molecules is mainly dependent on the movement of  $\text{OH}^-$ . During the water electrolysis process, the electronegative  $\text{OH}^-$  ions migrate towards the anode, while the electropositive  $\text{K}^+$  ions move towards the cathode. Thus, in low concentration of KOH (such as 1 M), the HBN shall be slightly disrupted (Fig. 3b), but water molecules still face a significant energy barrier from the HBN to reach the electrode surface. Additionally,  $\text{OH}^-$  ions at the electrode surface exert electrostatic repulsion, which carries away some water molecules. This explains the decreased water peak intensity observed in the in-situ Raman spectra for A100-6 during the hydrogen evolution reaction (HER) process in 1 M KOH. With high KOH concentrations, the increased  $\text{OH}^-$  ion concentration disrupts the HBN more significantly (Fig. 3c), which is reflected in the increased intensity of the peak at  $3600\text{ cm}^{-1}$  in the Raman spectra for both A100-6 and A100 in 6 M KOH. This higher disruption degree of

the HBN facilitates the movement of water molecules, which covers the effect from electrostatic repulsion of  $\text{OH}^-$  at the cathode. This explains the continuously increased water peak intensity observed in the in-situ Raman spectra for A100-6 during the HER process in 3 M and 6 M KOH.

On the other hand, during the OER process, the anode surface becomes positively charged due to the applied electric field, causing  $\text{OH}^-$  ions to migrate toward the anode under electrostatic force. This movement is opposite to that observed in the HER process. Additionally, owing to the strong hydrogen bonding between  $\text{OH}^-$  and water molecules, some water molecules also migrate toward the anode.<sup>33</sup> To further investigate the effect of the HBN on water molecule migration, in-situ Raman spectroscopy during the OER process was performed. As shown in Fig. S12 (ESI<sup>†</sup>), the increase in the Raman peak intensities of water molecules is observed for both A100-6 and A100 during the OER process, regardless of whether the KOH concentration is 1 M, 3 M, or 6 M.

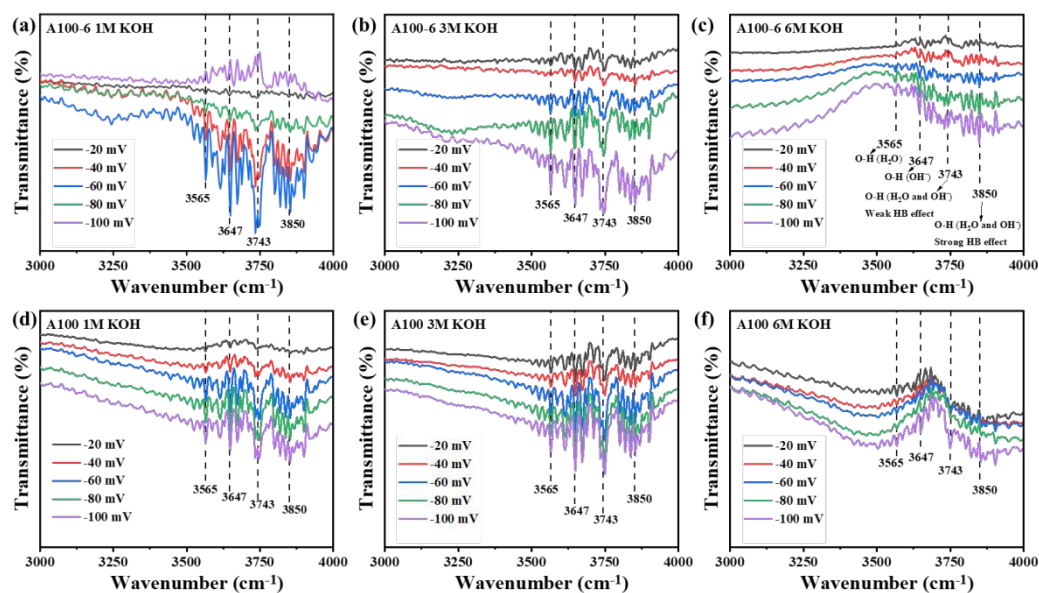


**Fig. 4** In-situ FTIR spectra (HER process) of A100-6 tested in (a) 1M KOH, (b) 3 M KOH and (c) 6 M KOH, respectively. In-situ FTIR spectra of A100 tested in (d) 1M KOH, (e) 3 M KOH and (f) 6 M KOH at different overpotentials, respectively.

In-situ Fourier transform infrared spectroscopy (FTIR) was conducted to further prove the HBN effect. As shown in Fig. 4, four apparent peaks can be found at  $3565$ ,  $3647$ ,  $3743$  and  $3850\text{ cm}^{-1}$ , which correspond to the O-H stretching of  $\text{H}_2\text{O}$ , O-H stretching of  $\text{OH}^-$ , O-H stretching with weak hydrogen bonding of  $\text{H}_2\text{O}$  and  $\text{OH}^-$ , and O-H stretching with strong hydrogen bonding of  $\text{H}_2\text{O}$  and  $\text{OH}^-$ , respectively.<sup>33–37</sup> For A100-6, the intensity of the transmission peaks in 1M KOH solution shows an overall decreasing trend with increasing voltage (Fig. 4a), while it increases in 3 M and 6 M KOH solutions (Figs. 4b and c). This suggests that the number of water molecules decreases with increasing voltage during the HER reaction in 1M KOH solution but increases in 3 M and 6 M KOH solutions, which is consistent with the results obtained from the in-situ Raman test. For A100, the intensity of the transmission peaks in 1M, 3 M, and 6 M KOH solutions consistently increases with increasing voltage (Figs. 4d–f). These trends agree with the observations

from the in-situ Raman tests. Moreover, in the HER process, the intensity of the spectroscopic signals obtained in both in-situ Raman and in-situ FTIR represents the number of active molecules. The HER processes of A100 and A100-6 in 1M KOH solution show opposite trends, which suggests that they do not have the same interaction with water molecules, and more specifically it can be attributed to the effect of the electrode surfaces of the two samples on hydrogen bonding network of water molecules in the solution. In conclusion, the correlation between the in-situ Raman and in-situ FTIR spectra clearly demonstrates the effect of HBN on  $\text{OH}^-$ -induced migration of water molecules.

In summary, the effects of the HBN on the migration of water molecules were systematically investigated on the A100 catalyst surface in various KOH electrolytes. A suppressed migration of water molecules as reactants was observed in 1 M KOH solution due to the relatively strong HBN, while promoted



ones in 3 M and 6 M KOH solutions. Such phenomena reveal the different HBN effects triggered by the influence of OH<sup>-</sup> with different concentrations of KOH. This study provides valuable insights into water transport kinetics and offers a pathway for optimizing industrial water electrolysis.

### Author contributions

Chengcheng Zhong (Conceptualization: Lead; Formal analysis: Lead; Investigation: Lead; Methodology: Lead; Writing -original draft: Lead); Yuxuan Xiao (Project administration: Equal; Writing -review & editing: Equal); Jinxian Feng (Software: equal; Visualization: equal); Chunfa Liu (Software: equal; Visualization: equal); Lun Li (Software: equal; Visualization: equal); Weng Fai IP (Funding acquisition: Supporting); Shuangpeng Wang (Funding acquisition: Supporting; Resources: Supporting); Hui Pan (Funding acquisition: Lead; Project administration: Equal; Supervision: Supporting; Writing -review & editing: Equal).

### Conflicts of interest

There are no conflicts to declare.

### Data availability

The data supporting this article have been included as part of the Supplementary Information.

### Acknowledgements

This work was supported by the Science and Technology Development Fund (FDCT) from Macau SAR (0050/2023/RIB2, 0023/2023/AFJ, 006/2022/ALC, 0087/2024/AFJ and 0111/2022/A2) and Multi-Year Research Grants (MYRG-GRG2024-00038-IAPME, and MYRG-GRG2023-00010-IAPME) from the University of Macau.

### References

- P. Zhou, P. Niu, J. Liu, N. Zhang, H. Bai, M. Chen, J. Feng, D. Liu, L. Wang and S. Chen, *Adv. Funct. Mater.*, 2022, **32**, 2202068.
- N. Farrell, *Renew. Sustain. Energy. Rev.*, 2023, **178**, 113216.
- F. Osselin, C. Soulaire, C. Fauguerolles, E. C. Gaucher, B. Scaillet and M. Pichavant, *Nat. Geosci.*, 2022, **15**, 765-769.
- M. K. Debe, *Nature*, 2012, **486**, 43-51.
- J.-H. Li, H.-Y. Zhang, Q.-W. Shi, J. Ying and C. Janiak, *Prog. Mater. Sci.*, 2024, **146**, 101335.
- J. Ying, M. D. Symes and X.-Y. Yang, *Matter*, 2023, **6**, 674-676.
- J. Ying, Y. Xiao, J. Chen, Z.-Y. Hu, G. Tian, G. V. Tendeloo, Y. Zhang, M. D. Symes, C. Janiak, and X.-Y. Yang, *Nano Lett.*, 2023, **23**, 7371-7378.
- Q. Lu, A. L. Wang, Y. Gong, W. Hao, H. Cheng, J. Chen, B. Li, N. Yang, W. Niu, J. Wang, Y. Yu, X. Zhang, Y. Chen, Z. Fan, X. J. Wu, J. Chen, J. Luo, S. Li, L. Gu and H. Zhang, *Nat. Chem.*, 2018, **10**, 456-461.
- C. G. Morales-Guio, L. A. Stern and X. Hu, *Chem. Soc. Rev.*, 2014, **43**, 6555-6569. DOI: 10.1039/D4TA08772K
- F. Yu, H. Zhou, Y. Huang, J. Sun, F. Qin, J. Bao, W. A. Goddard, S. Chen and Z. Ren, *Nat. Commun.*, 2018, **9**, 2551.
- T. Chen, C. Qiu, X. Zhang, H. Wang, J. Song, K. Zhang, T. Yang, Y. Zuo, Y. Yang, C. Gao, W. Xiao, Z. Jiang, Y. Wang, Y. Xiang and D. Xia, *J. Am. Chem. Soc.*, 2024, **146**, 1174-1184.
- C. Liu, J. Feng, P. Zhou, D. Liu, L. Qiao, D. Liu, Y. Cao, S.-C. Su, H. Liu and H. Pan, *Chem. Eng. J.*, 2023, **476**, 146710.
- Z.-H. Dong, Z. Jiang, T. Tang, Z.-C. Yao, D. Xue, S. Niu, J. Zhang and J.-S. Hu, *J. Mater. Chem. A.*, 2022, **10**, 12764-12787.
- S. Xu, Q. Wu, B.-A. Lu, T. Tang, J.-N. Zhang and J.-S. Hu, *Acta Phys.-Chim. Sin.*, 2023, **39**, 2209001.
- Z.-H. Yin, H. Liu, J.-S. Hu and J.-J. Wang, *Nati. Sci. Rev.*, 2024, **11**, nwae362.
- L. Zhai, T. W. Benedict Lo, Z.-L. Xu, J. Potter, J. Mo, X. Guo, C. C. Tang, S. C. Edman Tsang and S. P. Lau, *ACS Energy Lett.*, 2020, **5**, 2483-2491.
- S. Jeong, C. Huang, Z. Levell, R. X. Skalla, W. Hong, N. J. Escorcia, Y. Losovyj, B. Zhu, A. N. Butrum-Griffith, Y. Liu, C. W. Li, D. Reifsnnyder Hickey, Y. Liu and X. Ye, *J. Am. Chem. Soc.*, 2024, **146**, 4508-4520.
- J. Ying, Y. Xiao, J. Chen, Z.-Y. Hu, G. Tian, G. V. Tendeloo, Y. Zhang, M. D. Symes, C. Janiak and X.-Y. Yang, *Nano Lett.*, 2023, **23**, 7371-7378.
- J.-B. Chen, J. Ying, Y. Tian, Y.-X. Xiao and X.-Y. Yang, Electro catalysis under Magnetic Fields, *Adv. Funct. Mater.*, 2024, **24**, 2415660.
- J. Ying, S. Lenaerts, M. D. Symes and X.-Y. Yang, *Adv. Sci.*, 2022, **9**, e2106117.
- L. Su, J. Chen, F. Yang, P. Li, Y. Jin, W. Luo and S. Chen, *J. Am. Chem. Soc.*, 2023, **145**, 12051-12058.
- I. V. Stiofkin, C. WeeRaman, P. A. Pieniazek, F. Y. Shalhout, J. L. Skinner and A. V. Benderskii, *Nature*, 2011, **474**, 192-195.
- Y. Xu, Y.-B. Ma, F. Gu, S.-S. Yang and C.-S. Tian, *Nature*, 2023, **621**, 506-510.
- B. Huang, R. R. Rao, S. You, K. Hpone Myint, Y. Song, Y. Wang, W. Ding, L. Giordano, Y. Zhang, T. Wang, S. Muy, Y. Katayama, J. C. Grossman, A. P. Willard, K. Xu, Y. Jiang and Y. Shao-Horn, *JACS Au*, 2021, **1**, 1674-1687.
- J. Huang, M. Li, M. J. Eslamibidgoli, M. Eikerling and A. Gross, *JACS Au*, 2021, **1**, 1752-1765.
- P. Li, Y. Jiang, Y. Hu, Y. Men, Y. Liu, W. Cai and S. Chen, *Nat. Cat.*, 2022, **5**, 900-911.
- O. van der Heijden, S. Park, R. E. Vos, J. J. J. Eggebeen and M. T. M. Koper, *ACS Energy Lett.*, 2024, **9**, 1871-1879.
- S. Niu, T. Tang, Y. Qu, Y. Chen, H. Luo, H. Pan, W.-J. Jiang, J. Zhang and J.-S. Hu, *CCS Chem.*, 2024, **6**, 137-148.
- G. P. Pavithra and A. C. Hegde, *Appl. Surf. Sci.*, 2012, **258**, 6884-6890.
- Y.-X. Xiao, J. Ying, J.-B. Chen, X. Yang, G. Tian, J.-H. Li, C. Janiak and X.-Y. Yang, *Adv. Funct. Mater.*, 2024, **24**, 2418264.
- K. Hedenstedt, J. Bäckström and E. Ahlberg, *J. Electrochem. Soc.*, 2017, **164**, H621-H627.





## COMMUNICATION

Journal Name

- 32 M. Sbroscia, A. Sodo, F. Bruni, T. Corridoni and M. A. Ricci, *J. Phys. Chem. B*, 2018, **122**, 4077-4082.
- 33 P.-Y. Wang, J.-F. Zhou, H. Chen, B. Peng and K. Zhang, *JACS Au*, 2022, **2**, 1457-1471.
- 34 X. Zhang, Y. Xu, Y. Zhou, Y. Gong, Y. Huang and C. Q. Sun, *Appl. Surf. Sci.*, 2017, **422**, 475-481.
- 35 N. Agmon, H. J. Bakker, R. K. Campen, R. H. Henchman, P. Pohl, S. Roke, M. Thamer and A. Hassanali, *Chem. Rev.*, 2016, **116**, 7642-7672.
- 36 C. J. Fecko, J. D. Eaves, J. J. Loparo, A. Tokmakoff and P. L. Geissler, *Science*, 2003, **301**, 1698-1702.
- 37 K. Mizuse, N. Mikami and A. Fujii, *Angew. Chem. Int. Ed.*, 2010, **49**, 10119-10122.

View Article Online  
DOI: 10.1039/D4TA08772K

Open Access Article. Published on 27 February 2025. Downloaded on 2/27/2025 10:34:32 PM.  
This article is licensed under a Creative Commons Attribution-NonCommercial 3.0 Unported Licence.



Journal of Materials Chemistry A Accepted Manuscript

## Data Availability Statement

View Article Online  
DOI: 10.1039/D4TA08772K

The data that support the findings of this study are available in the supplementary material of this article.

